IEEE Access
Multidisciplinary ⋮ Rapid Review ⋮ Open Access Journal

Received September 3, 2018, accepted October 22, 2018, date of publication October 29, 2018,
date of current version November 19, 2018.

Digital Object Identifier 10.1109/ACCESS.2018.2878423

Multi-Sensor Obstacle Detection System Via Model-Based State-Feedback Control in Smart Cane Design for the Visually Challenged

NUR SYAZREEN AHMAD, (Member, IEEE), NG LAI BOON, AND PATRICK GOH
School of Electrical and Electronic Engineering, Engineering Campus, Universiti Sains Malaysia, Nibong Tebal 14300, Malaysia.
Corresponding author: Nur Syazreen Ahmad (syazreen@usm.my)

This work was supported by the Ministry of Education of Malaysia through the FRGS Scheme under Grant 203/PELECT/6071347.

ABSTRACT Smart canes are usually developed to alert visually challenged users of any obstacles beyond the canes' physical lengths. The accuracy of the sensors and their actuators' positions are equally crucial to estimate the locations of the obstacles with respect to the users so as to ensure only correct signals are sent through the associated audio or tactile feedbacks. For implementations with low-cost sensors, however, the users are very likely to get false alerts due to the effects from noise and their erratic readings, and the performance degradation will be more noticeable when the positional fluctuations of the actuators get amplified. In this paper, a multi-sensor obstacle detection system for a smart cane is proposed via a model-based state-feedback control strategy to regulate the detection angle of the sensors and minimize the false alerts to the user. In this approach, the overall system is first restructured into a suitable state-space model, and a linear quadratic regulator (LQR)-based controller is then synthesized to further optimize the actuator's control actions while ensuring its position tracking. We also integrate dynamic feedback compensators into the design to increase the accuracy of the user alerts. The performance of the resulting feedback system was evaluated via a series of real-time experiments, and we showed that the proposed method provides significant improvements over conventional methods in terms of error reductions.

INDEX TERMS Multi-sensor, visually challenged, model-based control, state-feedback, obstacle detections.

I. INTRODUCTION

White canes are universally recognized as symbols of blind people, and they have been used since the 1920s as mobility aids to guide users while walking or navigating particularly in unfamiliar places [1]. Other than their basic function which is to give the users tactile information about the environment such as obstacles on the ground, holes and uneven surfaces, most of them are designed in such a way that they are light and retractable or foldable, which can increase the travel convenience of the users. Nevertheless, these traditional travel aids only have short sensing ranges which limit the obstacle detections below the knee levels and require the canes to physically bump into the objects to alert the users. Due to these limitations, electronic travel aids (ETAs) were introduced in the 1970s [1]–[3], not just to extend the sensing range, but also to promote a safer and more confident independent walking experience.

Sensor technology is one of the most important factors that can enhance the performance of the ETAs. Smart cane device is a type of ETA which is typically designed to fit on top of the white cane for obstacle detections above-knee levels. This device is intended to help the visually challenged to engage in a safe and efficient independent travel by increasing the user access to certain categories of environmental information. The most common technologies that are used for distance measurements from obstacles include infrared (IR) sensors which transmit IR lights towards the objects, sonar sensors which use high-frequency sound waves in place of IR lights, and laser rangefinders which produce laser waves for the same purpose. The IR sensor technology works by measuring the signal strength to estimate the distance. The advantages of IR sensors over other sensor types are faster response, narrow range and high resolution which makes them more suited for small distance measurement [4], [5]. The accuracy of this type of sensor however is affected by the reflectivity and color of the objects due to its dependence on signal strength. As it is also very sensitive to the sunlight, its reading can vary if the luminance in the environment changes [6]. This drawback however is not an issue to the sonar and laser range finders which share a similar working principle commonly known as Time-of-Flight (ToF). This principle leads to a simple mathematical calculation for distance measurement from the sensor to the object, that is, by generating a beam of energy waves directed towards an object, the time it takes for the beam to make its journey back towards its source after being reflected can be used to estimate the distance traveled. As laser beam offers a distinct advantage of being able to travel many times faster than that provided by sonar sensors, it is often used to detect both static and moving objects [7]. In [8], a fusion of a laser sensor and a camera for an electronic virtual white cane implementation was proposed where the distance calculation was based on the laser's position and the image captured. Nevertheless, for simple design goals, some preferred to avoid using this kind of technology as the laser light is known to be harmful to humans, and extra precautions are required when using them [9]. The sonar technology, on the other hand, despite its low resolution and slower response as compared to IR and laser, is still being preferred by many developers and has become among the most common sensing technique for mobility aids. This is mainly due to its low-cost and broad beam-width which allows for a wide detection range [1], [10].

As the sensor technology is rapidly evolving in parallel with the emerging trends in Internet-of-Things (IoT) and embedded systems, many refinements of the early ETAs with new innovative technologies have been developed in modern assistive devices [11]. Integration of multiples sensors on a single platform to overcome the limitations of individual sensors has become increasingly popular in recent years [4], [12]–[17]. Combinations of multiple ultrasonic and other sensors have been reported in a series of papers [13], [15], [17], [18] to accommodate a wider range of obstacles and sensing area. There is also a growing number of recent studies on microcontroller-based assistive devices which allow faster user alerts via various types of actuators and wireless feedbacks. Vibrators, for instance, are extensively used to provide haptic or vibrotactile feedbacks with different intensities [14], [19], [20]. Another interesting approach by [21] and [22] where steering actions of a mini wheeled mobile robot attached to a white cane was introduced to provide a vibrotactile feedback with a sense of direction. Apart from that, audio voice/texts or acoustic feedbacks have also been considered by many researchers which can alert the users wirelessly through smartphones and/or headsets [16], [18], [20], [21], [23]–[26].

Despite the technological revolution, the assistive devices have not been successfully adopted and used by a large number of people with visual impairments, and many still prefer to use the white canes [27], [28]. Several research findings have shown issues related to the limited use of these smart devices, which include high prices, safety, orientations, speed, mobility, portability and optimizations of techniques [28], [29]. Combinations of many different sensors, for instance, although faster feedback and wider detection range can be achieved, the size and power consumption of the device will also increase which directly affect the price, portability and mobility of the device. For some cases, a lot of variations in the user alerts may be confusing and less intuitive, and users usually prefer to receive simplified signals without having to process a lot of raw data from the feedbacks. These issues have sparked a growing interest among researchers to study on the design guidelines and improvements that can be introduced to increase the usability and marketibility of the devices [10], [11], [28].

Inspired by a number of recent smart cane configurations [6], [14], [15], a simple design with integration of ultrasonic and IR sensors for obstacles detection, and vibrotactile and audio techniques for the feedbacks has been implemented for the prototype smart cane in this work. The sensors are positioned in such a way that the sensing range of the ultrasonic sensors includes the left and right front of the user, and from the ground level to the head level, while the IR sensor is used for uneven ground surface detection such as holes and descending stairs. Since the device involves low-cost sensors, the signals sent to the user are prone to noise and erratic readings which may lead to false alarms, and the performance will become worse when the sensors' positions oscillate with the user's hand movements. As suggested in [28], the horizontal orientation of the cane can be fixed by including a mark or indicator on the handlebar to ensure the sensors are always facing forward. While this can be controlled by the user, the sensors' vertical detection angle is bound to fluctuate since the user usually has to tilt the cane back and forth while walking. Motivated by these issues, the focus of this work is on improvement of the obstacle detection system by means of model-based state feedback technique. In this approach, the overall system is first restructured into a suitable state-space model which also includes an accelerometer to sense the tilt angle. A motorized actuator is used to control the vertical detection angle of the ultrasonic sensors, and a linear quadratic regulator (LQR)-based controller is synthesized to further optimize the actuator's control actions while ensuring its position tracking. We also integrate dynamic feedback compensators into the design which additionally act as noise filters to increase the accuracy of the user alerts. The performance of the resulting feedback system was evaluated via a series of real-time experiments, and we showed that the proposed method provides significant improvements over the conventional methods in terms of error reductions.

II. METHODOLOGY AND MAIN RESULTS

The overall view of the smart cane system configuration is depicted as in Figure 1 where five sensors (one accelerometer, S_a, three ultrasonic sensors S_h, S_{mr}, S_{ml} and one infrared sensor, S_g) serve as the interface for input signals to an ATmega328p microcontroller, a servo motor to control the sensors' positions, a vibration motor for the vibrotactile alert, and a bluetooth module for wireless audio feedback. The focus of this work is on improving the performance of the user alerts which rely on the accuracy of the sensors' positions

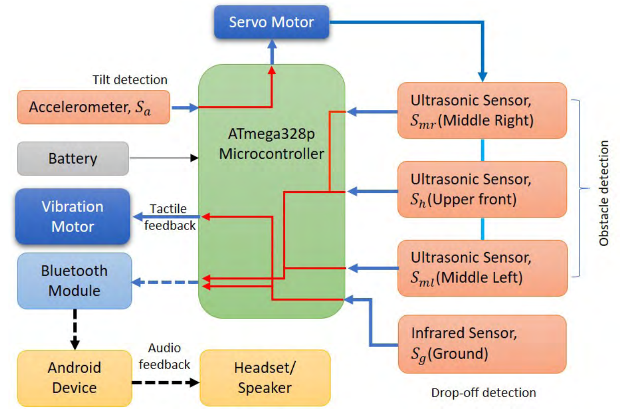

FIGURE 1. Overview of the smart cane system architecture. The scope of this work is highlighted by the solid blue and red arrows which represent the signals to/from actuators/sensors and control algorithms respectively.

and readings. These are highlighted by the blue arrows signals as in the figure, and the red arrows which also indicate the associated control algorithms.

The sensors S_a, S_h, S_{mr}, S_{ml} are attached to a smart cane (SC) board, and are positioned in such a way that any obstacles from the head level to the ground level in front of the user can be detected. The sketch of the detection range is illustrated in Figure 2 together with S_g for the drop-off detection at the ground level. Appropriate signals can then be transmitted to the user via vibrotactile and wireless audio feedbacks to an Android device and headset/speaker via bluetooth for obstacle detection alerts.

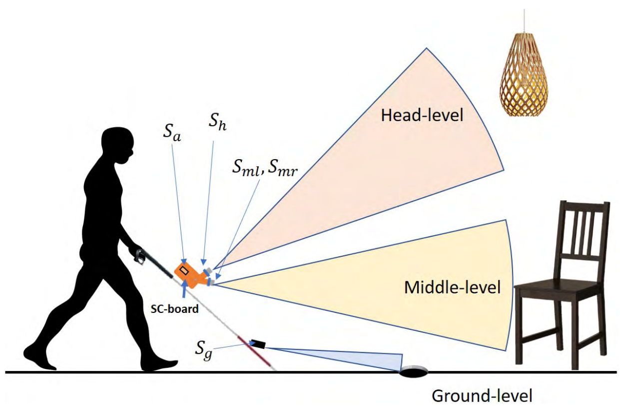

FIGURE 2. Sketch of obstacle and drop-off detection range with three-leveled sensors (S_a, S_g, S_{ml}, S_{mr} and S_h).

In what follows, we present an equivalent open-loop model of the SC system in state space domain which is restructured to pave the way for model-based state-feedback control design. The notations used throughout this paper are listed in Table 1.

A. OPEN-LOOP SYSTEM MODELLING

With reference to Figure 3, define $\mathbf{x_1} = [x_{11}\ x_{12}]^T$ where x_{11} and x_{12} represent the servo's angle and accelerometer's

TABLE 1. Notations used in this work.

Notation	Definition
$\mathbb{R}$	fields of any real numbers
$\mathbb{R}^+$	fields of positive real numbers
$\mathbb{R}^-$	fields of negative real numbers
$\mathbb{R}^{n\times p}$	fields of real $n \times p$ matrices
$\mathbb{Z}^+$	fields of positive integers
$0_{m\times n}$	a zero $m \times n$ matrix
$x, \dot{x}$	$x(t)$, $dx(t)/dt$
$\mathscr{L}\{x(t)\}$	Laplace transform of $x(t)$ defined for $t \in [0, \infty)$
$\mathbb{RH}_\infty^{n\times m}$	set of all proper and real rational stable transfer function matrices with n rows and m columns
$(x_1, x_2, x_3) \le (\varepsilon_1, \varepsilon_2, \varepsilon_3)$	element-by-element inequality, $x_i \le \varepsilon_i$

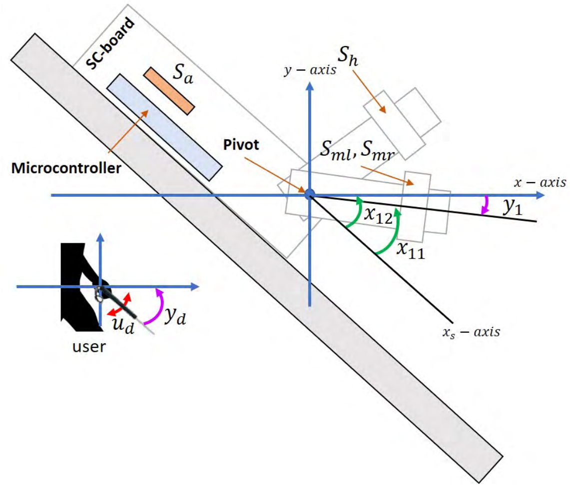

FIGURE 3. System modelling for the signals around the SC board.

angle with respect to x_s-axis respectively. The distances of S_{ml}, S_{mr} and S_h from obstacles as illustrated in Figure 4 are written as $\mathbf{x_2} \in \mathbb{R}^3$ with $\mathbf{x_2} = [x_{21}\ x_{22}\ x_{23}]^T$, and the distance of S_g from the drop-off location as $x_3 \in \mathbb{R}$. The state-vector can then be represented by $\mathbf{x_o} = [\mathbf{x_1}\ \mathbf{x_2}\ x_3]^T$. The angles θ_h, θ_m and θ_g are fixed and can be adjusted according to the user's height or convenience. As for the outputs, let y_1, y_2, y_3 and y_d represent the servo's angle w.r.t the x-axis, the input to serial communication via bluetooth for voice alert, the input to the vibration motor (tactile feedback), and the smart cane's angle with respect to x_s-axis respectively. The inputs to the system will be u_1 (input to the servo), $\mathbf{u_{02}} = [u_{21}\ u_{22}\ u_{23}]^T$ (input signals to S_{ml}, S_{mr} and S_h respectively), u_{03} (input signal to S_g) and u_d (user's movement).

The open-loop system can then be written as

$$\dot{\mathbf{x}_o} = A\mathbf{x_o} + B\mathbf{u_o} \tag{1}$$

$$\mathbf{y_o} = C\mathbf{x_o} + D\mathbf{u_o} \tag{2}$$

where

$$A = \begin{bmatrix} A_1 & 0 & 0 \\ 0 & 0 & 0 \\ 0 & 0 & 0 \end{bmatrix}, \quad B = \begin{bmatrix} B_1 & 0 & 0 & B_d \\ 0 & 0 & 0 & 0 \\ 0 & 0 & 0 & 0 \end{bmatrix},$$

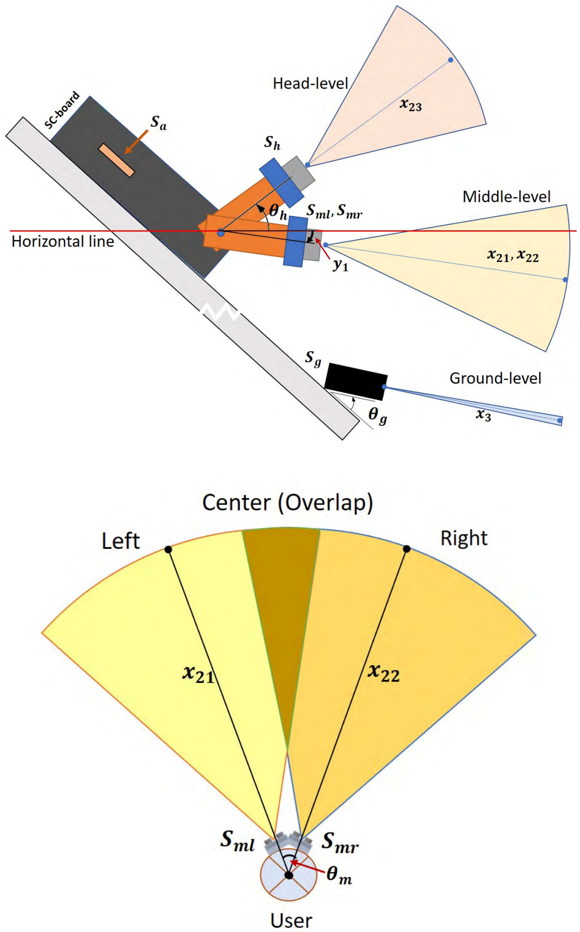

FIGURE 4. Close-up on the side view (top) and top view (bottom) of the smart cane system with the sketch of its detection range.

$$C = \begin{bmatrix} C_1 & 0 & 0 \\ 0 & C_2 & 0 \\ 0 & 0 & C_3 \\ C_d & 0 & 0 \end{bmatrix}, \quad D = 0_{4\times 4}$$

$$\mathbf{y_o} = [y_1 \quad y_2 \quad y_3 \quad y_d]^T, \quad \mathbf{u_o} = [u_1 \quad \mathbf{u_{02}} \quad u_{03} \quad u_d]^T; \tag{3}$$

with $A_1 \in \mathbb{R}^{2\times 2}, B_1 \in \mathbb{R}^{2\times 1}, C_1, C_d \in \mathbb{R}^{1\times 2}, B_d, C_2 \in \mathbb{R}^{1\times 3}$ and $C_3 \in \mathbb{R}$. The matrices A_1, B_1, C_1, C_2 and C_3 depend on the model of the main actuator and the sensors, while B_d and C_d rely on the user's hand movement. It is also straightforward that $C_d = [0\ \gamma]$, $\gamma \in \mathbb{R}$, as the orientation of S_a is parallel with the SC-board's.

Although servo motors generally provide a perfect steady-state tracking particularly for step responses, with the ultrasonic sensors and other load attached, their dynamic will be slightly affected. Moreover, as the nature of the inputs is always uncertain and highly depends on the user's movement, it is therefore useful to take into account the actuator's dynamic in order to ensure the tracking behaviour stays within the desired specifications. From the system's architecture, we can write the main actuator as a subsystem G_a, i.e.

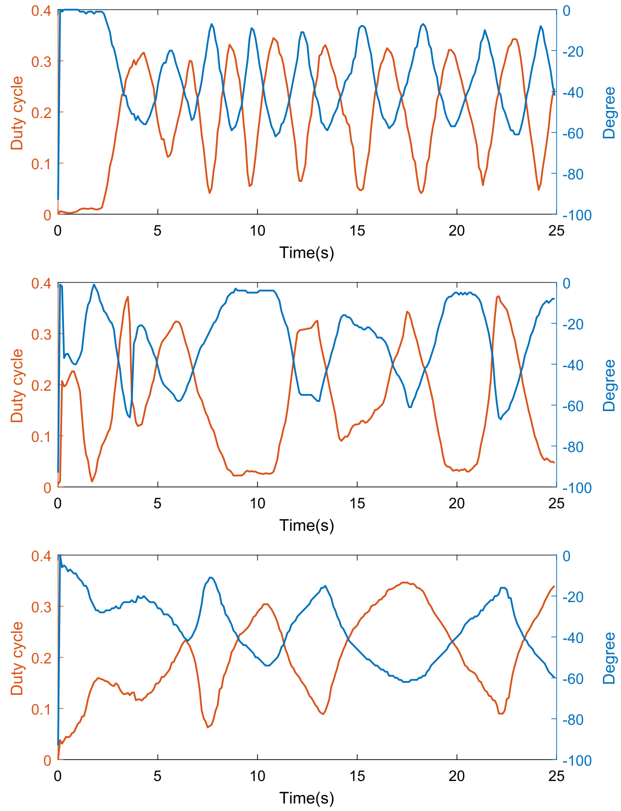

FIGURE 5. Open-loop response of the system G_a without any state-feedback for three different scenario; Movement 1 (top), Movement 2 (middle) and Movement 3 (bottom). The orange line represents the duty cycle of u_1, and the light blue line represents y_1.

$$G_a \sim (A_1, B_1, C_1, 0);$$
$$A_1 = \begin{bmatrix} A_{11} & 0 \\ 0 & 0 \end{bmatrix}, \quad B_1 = \begin{bmatrix} B_{11} \\ 0 \end{bmatrix}, \quad C_1 = [1 \quad -1] \tag{4}$$

Without any state feedback, the first state cannot be controlled at all. Assuming $x_{11} = \alpha$ where $\alpha \in \mathbb{R}$ is a constant, the uncontrolled output y_1 then reduces to $y_1 = \alpha - x_{12}$. If $\alpha = 0$ for instance, the output will be the inverse of the accelerometer's angle from the x_s-axis. In order to estimate the state-space model of the main actuator, three different control input profiles which represent the responses from the servo motor based on three different user movements were fed into the system, and the outputs were then compared with the inputs as shown in Figure 5. Via the open-loop model, the user can also be alerted of the obstacle's position and drop-off through $\mathbf{x_2}$ and x_3. For instance, setting $C_3 = 1$, a warning to the user for the drop-off can be delivered via y_3 which then activates the vibrator. As for the obstacle positions, the alerts via y_2 will be sent to the user via wireless serial transmit, hence discretized signals for the audio feedbacks are more suitable. This can be acheived by assigning

$$x_{2i} = \begin{cases} 1 & \text{when } u_{2i} \neq 0 \\ 0 & \text{when } u_{2i} = 0 \end{cases} \tag{5}$$

for $i = 1, 2, 3$ and $C_2 = [1\ 2\ 4]$. The relationship between $\mathbf{x_2}$ and y_2 along with the user alert is summarized in Table 2.

TABLE 2. User alert of the obstacle's position via open-loop control.

x_{21}	x_{22}	x_{23}	y_2	User alert (obstacle's position)
0	0	0	0	none
1	1	1	7	center (high)
1	1	0	3	center
0	0	1	4	center (hang)
0	1	0	2	right
0	1	1	6	right (high)
1	0	0	1	left
1	0	1	5	left (high)

Although the abovesaid methods can be easily implemented, the users are very likely to get false alerts due to fluctuations of detection areas, along with noise and erratic readings from the sensors. In the next subsection, we introduce a model-based state-feedback control design to enhance the performance of the smart cane system by minimizing the false alerts to the users.

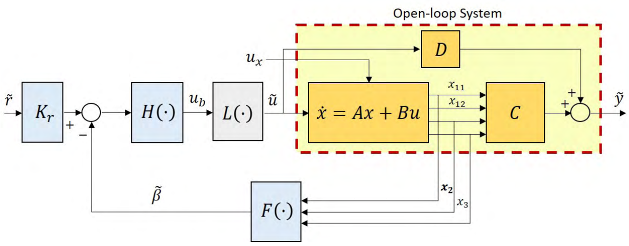

FIGURE 6. Proposed model with state-feedback control strategy.

B. MODEL-BASED STATE FEEDBACK CONTROL DESIGN

In this work, it is desired that the angle of the main actuator stays at an optimal point (i.e. slightly below the x-axis) to ensure accurate obstacle position detection, and the outputs of the microcontroller which are fed to the vibration motor and bluetooth module are able to alert the user on any obstacles and drop-off ahead. To this end, a state-feedback approach is introduced as shown in Figure 6. It is worth noting that, from the open-loop model in (1)-(3), only y_1, y_2 and y_3 can be regulated by the microcontroller, and the exogenous signal $u_x = [\mathbf{u_{02}}\ u_{03}\ u_d]^T$ depends on the user and inputs to the sensors. In this state-feedback design, another new output, y_4, is augmented to send a signal when the obstacle is within a predefined distance (the detail is in requirement (A2) below) from the user. As this entails a new control scheme to detect the obstacle's position, a new control input vector $\tilde{u}$ is introduced. The new output and control input vectors can then be formed as $\tilde{y} = [y_1\ y_2\ y_3\ y_4]^T$ and $\tilde{u} = [u_1\ u_2\ u_3\ u_4]^T$ respectively, which results in the following state space matrices:

$$\tilde{A} = \begin{bmatrix} A_1 & 0_{2\times2} \\ 0_{2\times2} & 0_{2\times2} \end{bmatrix}, \quad \tilde{B} = \begin{bmatrix} B_1 & 0_{2\times3} \\ 0_{2\times1} & 0_{2\times3} \end{bmatrix},$$

$$\tilde{C} = \begin{bmatrix} C_1 & 0_{1\times2} \\ 0_{3\times2} & 0_{3\times2} \end{bmatrix}, \quad \tilde{D} = \begin{bmatrix} 0 & 0 & 0 & 0 \\ 0 & D_2 & 0 & 0 \\ 0 & 0 & D_3 & 0 \\ 0 & 0 & 0 & D_4 \end{bmatrix} \tag{6}$$

with $A_1 \in \mathbb{R}^{2\times2}$, $B_1 \in \mathbb{R}^{2\times1}$, $C_1, \in \mathbb{R}^{1\times2}$, $D_2, D_3 \in \mathbb{R}$ and $D_4 \in \mathbb{R}^3$. The main compensators are represented by

$$K_r \in \mathbb{R}^{3\times3}; \quad F = \begin{bmatrix} F_1 & 0 & 0 \\ 0 & F_2 & 0 \\ 0 & 0 & F_3 \end{bmatrix} \quad \text{and}$$

$$H = \begin{bmatrix} H_1 & 0 & 0 \\ 0 & \Phi_2 & 0 \\ 0 & 0 & \Phi_3 \\ 0 & \Phi_4 & 0 \end{bmatrix}. \tag{7}$$

with $F_1, H_1 \in \mathbb{R}$, $F_2, F_3 \in \mathbb{RH}_\infty^{3\times3}$, and $\Phi_2, \Phi_3, \Phi_4 : \mathbb{R}^3 \to \mathbb{R}$. Apart from that, the limitation of the actuator, $L = diag(\phi_L, 1, 1, 1)$, is also included to accurately model the system. This gives $\tilde{u} = [\phi_L(u_{b1})\ u_{b2}\ u_{b3}\ u_{b4}]^T$ where $\phi_L : \mathbb{R} \to \mathbb{R}$ represents the constraint of the main actuator, i.e.

$$u_1 = \phi_L(u_{b1}) = \begin{cases} 0 & \text{for } u_{b1} < 0 \\ u_{b1} & \text{for } 0 \le u_{b1} \le 180 \\ 180 & \text{for } u_{b1} > 180. \end{cases} \tag{8}$$

1) DESIGN SPECIFICATIONS AND CONTROLLER SYNTHESIS

Let $\tilde{r} = [r_1\ \mathbf{r_2}\ r_3]^T$, $K_r = diag(K_1, K_2, K_3)$ and define the output of controller F as $\tilde{\beta} = [\beta_1\ \beta_2\ \beta_3]^T$. It is desired that y_1 tracks the reference at r_1 when the SC-board's orientation fluctuates between 0° and −90° from the x-axis. In order to achieve this, the following method is proposed:

Result 1: Consider the proposed closed-loop model as depicted in Figure 6, let $H_1 = 1$, $R_1(s) = \mathscr{L}\{r_1(t)\} = v/s$ where $v \in \mathbb{R}^-$ is the angle in degree, and $G_1 \sim (A_{11}, B_{11}, C_{11}, 0)$ with $C_{11} = 1$. Define the quadratic cost function as

$$J = \int_0^\infty (x_{11}^T Q x_{11} + u_{b1}^T R u_{b1})\, dt \tag{9}$$

where $Q, R \in \mathbb{R}^+$. The angle of the main actuator, y_1 will track its reference at r_1 with controllers F_1 and K_1 which can be designed with

$$F_1 = R^{-1} B_{11}^T P \quad \text{and } K_1 = G_{c1}(0)^{-1} \tag{10}$$

where $P \in \mathbb{R}^+$ satisfies

$$A_{11}^T P + P A_{11} - P B_{11} R^{-1} B_{11}^T P + Q = 0 \tag{11}$$

and

$$G_{c1}(s) = C_{11}(sI - (A_{11} - B_{11}F_1))^{-1} B_{11} \tag{12}$$

Proof: The transfer function $G_1(s)$ corresponds to the subsystem of the feedback loop for the state x_{11}. With $K_1 = 0$ and $H_1 = 1$, the system reduces to a standard state-feedback control framework where the control law F_1 can be designed by selecting appropriate values of Q and R and minimizing the cost function (9). The latter can also be simplified by solving (11) [30]. The perfect reference tracking can then be achieved by including $K_1 \in \mathbb{R}^+$ where

$$K_1^{-1} = \lim_{s \to 0} sG_{c1}(s)R(s), \tag{13}$$

which is also equivalent to the second equation in (10). □

Other than ensuring the reference tracking for the main actuator to minimize its positional fluctuations, it is also desired that

(A1) the user is notified of the obstacles' positions via y_2 and any drop-offs via y_3;
(A2) the user is alerted when the obstacle is within 50cm to 80cm via y_4 to provide a comfortable stopping distance at a normal walking speed;
(A3) the effects of $\mathbf{x}_2$ on y_2 from any fast moving object that is not approaching the user must be suppressed;
(A4) the number of false alerts is smaller than that from the open-loop approach.

In this regard, we propose the following control algorithm.

Result 2: Let $D_2 = D_3 = D_4 = 1$, $F_2 \sim (A_{f2}, B_{f2}, C_{f2}, D_{f2})$ and $F_3 \sim (A_{f3}, B_{f3}, C_{f3}, D_{f3})$ be designed such that eig $(A_{fi}) \in \mathbb{R}^-$,$|A_{fi}| \geq 0.5$, $F_i(0) = 1$ for $i = 1, 2$, $\beta_3 = F_3 x_3$ and $\beta_2 = F_2 \mathbf{x_2}$ with $\beta_2 = [\beta_{21}\ \beta_{22}\ \beta_{23}]^T$. Also, write $\mathbf{r_2} = [0\ 0\ 0]^T$ and $r_3 = 0$ so that

$$u_{b2} = -\Phi_2(\beta_2), \quad u_{b3} = -\Phi_3(\beta_3) \text{ and } u_{b4} = -\Phi_4(\beta_2) \tag{14}$$

If Φ_2, Φ_3 and Φ_4 satisfy the following constraints

$$-\Phi_2(\beta_2) = \begin{cases} 0 & \text{if } \beta_{2i} \leq \epsilon \quad \forall i = 1,2,3 \\ 7 & \text{if } -\beta_{2i} \leq -\epsilon \quad \forall i = 1,2,3 \\ 6 & \text{if } (\beta_{21}, -\beta_{22}, -\beta_{23}) \leq (\epsilon, -\epsilon, -\epsilon) \\ 5 & \text{if } (-\beta_{21}, \beta_{22}, -\beta_{23}) \leq (-\epsilon, \epsilon, -\epsilon) \\ 4 & \text{if } (\beta_{21}, \beta_{22}, -\beta_{23}) \leq (\epsilon, \epsilon, -\epsilon) \\ 3 & \text{if } (-\beta_{21}, -\beta_{22}, \beta_{23}) \leq (-\epsilon, -\epsilon, \epsilon) \\ 2 & \text{if } (\beta_{21}, -\beta_{22}, \beta_{23}) \leq (\epsilon, -\epsilon, \epsilon) \\ 1 & \text{if } (-\beta_{21}, \beta_{22}, \beta_{23}) \leq (-\epsilon_2, \epsilon_1, \epsilon_1) \end{cases} \tag{15}$$

$$-\Phi_3(\beta_3) = \begin{cases} 1 & \text{if } \beta_3 > 0 \\ 0 & \text{otherwise.} \end{cases} \tag{16}$$

$$-\Phi_4(\beta_2) = \begin{cases} 1 & \text{if } 50 - \epsilon_l < \beta_{2i} < 80 - \epsilon_u \text{ for any } i \\ 0 & \text{otherwise.} \end{cases} \tag{17}$$

where $\epsilon \in [25, 40]$ and $\epsilon_l, \epsilon_u \in [10, 30]$, the outputs y_2, y_3 and y_4 can be controlled to meet the design requirements as described in (A1)-(A4).

Proof: From the parameters of $\tilde{D}$ and algorithms for u_{b2}, u_{b3} and u_{b4}, the requirements (A1) and (A2) can be clearly met. In order to satisfy (A3) and (A4), F_2 and F_3 are designed such that the output maintains its stability (via eig $(A_{fi}) \in \mathbb{R}^-$ and $F_i(0) = 1$), and the false alerts due to the noise/erratic readings from the sensors can be minimized by delaying the output response with $|A_{fi}| \geq 0.5$. Also, due to the dynamic properties of F_2 and F_3, the threshold values of ϵ, ϵ_l and ϵ_u are included which can be selected after the system calibrations. □

TABLE 3. Accuracy (%) of the estimated model based on three different movements. M1, M2 and M3 denote Movements 1,2 and 3 respectively.

Model (A_{11}, B_{11})	M1 (%)	M2 (%)	M3 (%)	Average (%)
$(-3214, 31.77)$	98	98	97.84	97.84
$(-91.04, 89.94)$	98	97.89	97.85	97.91
$(-78.67, 77.17)$	98	97.99	97.85	**97.95**

III. NUMERICAL AND EXPERIMENTAL RESULTS

A. SYSTEM MODELLING FOR THE MAIN ACTUATOR

Three types of movements as explained in Section II-A have been considered in this work. The corresponding responses as shown in Figure 5 were compared via MATLAB System Identification Toolbox to estimate the parameters A_{11} and B_{11}. For each movement, estimated values of A_{11} and B_{11} were generated, and the accuracy of the response for each (A_{11}, B_{11}) pair was compared for each case. The results were summarized in Table 3. From the table, the estimated model with the highest accuracy on average is given by $(A_{11}, B_{11}) = (-78.67, 77.17)$. The responses of y_1 in open-loop via this estimated model (simulation) and experiment for the three types of movements are shown in Figure 7.

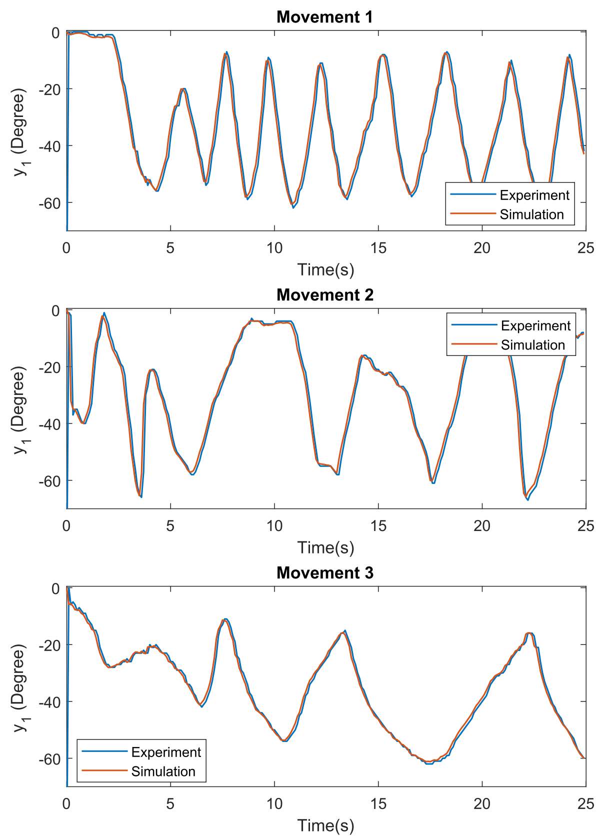

FIGURE 7. Comparison of the output y_1 in open-loop via simulation and experiment.

B. CONTROL SYNTHESIS AND PERFORMANCE EVALUATIONS

Applying Result 1 with $Q = 1.1$ and $R = 0.2$ to the best estimated model from Table 3, we obtained an optimized

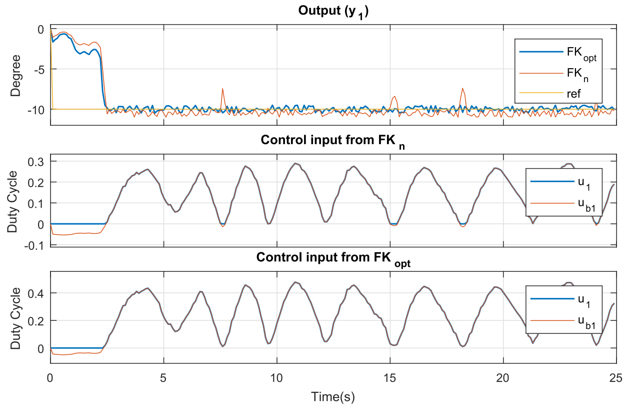

FIGURE 8. Output y_1 from the experiment with corresponding duty cycles for Movement 1. Both methods show a large overshoot due to unstable movement of the user at the beginning (at $t \leq 3$s). Slightly larger overshoots are seen from the response of FK_n at $t \approx 7.5$s, $t \approx 15.5$s and $t \approx 18$s.

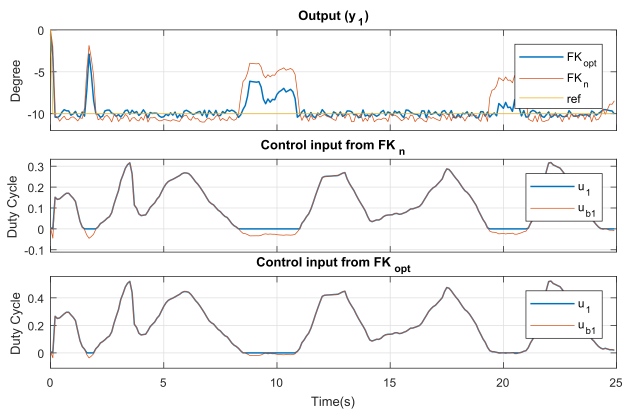

FIGURE 9. Output y_1 from the experiment with corresponding duty cycles for Movement 2. Larger overshoots are seen from the response of FK_n due to the duty cycles which go beyond the limits (at $t \approx 2$s, $t \in (8, 11)$s and $t \in (19, 21)$s).

compensator with $F_1 = 1.5378$ and $K_1 = 2.5572$. In order to test the position tracking performance of the main actuator, a suitable angle of $v = -10°$ was selected. The responses of y_1 with respect to Movements 1,2 and 3 together with the corresponding duty cycles (which map (0, 1) to (0°, 180°)) are illustrated in Figures 8, 9 and 10 respectively. The yellow line (i.e. *ref*) represents $r_1 = v$ whereas FK_{opt} and FK_n denote the y_1 responses via the optimized and non-optimized (i.e. $K_1 = 1$, and $F_1 = 1$) compensators respectively. From the figures, it is observed that both methods are generally able regulate the output at r_1. However, relatively larger positional fluctuations can be seen from the response via FK_n for each movement. This is mainly due to the non-optimized duty cycles (or control signals) which go beyond the ϕ_L limits for a certain period of time during the movements. The responses via FK_{opt} on the other hand show a significant improvement as the compensator's parameters have been optimized to ensure the duty cycles stay within the constraints for all movements. The corresponding integral of absoulte

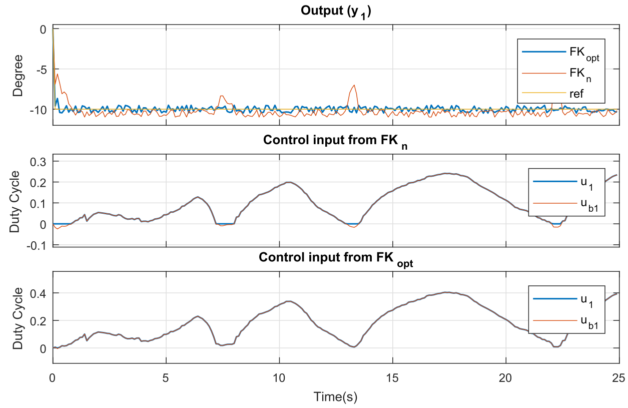

FIGURE 10. Output y_1 from the experiment with corresponding duty cycles for Movement 3. Slightly larger overshoots are seen from the response of FK_n at $t \in (0, 1)$s, $t \in (7, 8)$s and $t \in (13, 14)$s.

errors (IAEs), i.e.

$$IAE = \int_0^\infty |e(t)|dt, \quad e(t) = r_1(t) - y_1(t) \tag{18}$$

are summarized in Table 4, and it can also be concluded that the method proposed in Result 1 provides a significant reduction in terms of the position errors.

TABLE 4. Performance evaluation for the response of y_1 via optimized and non-optimized compensators.

	IAE (rad)		
Compensator	**Movement 1**	**Movement 2**	**Movement 3**
FK_n	5.53	5.67	2.79
FK_{opt}	4.01	2.55	1.12

With regard to the obstacle avoidance, the controllers F_2 and F_3 have been designed via Result 2 with

$$A_{f3} = -1.5, \quad B_{f3} = 1.5, \quad C_{f3} = 1; \quad D_{f3} = 0; \tag{19}$$

$$A_{f2} = \begin{bmatrix} -0.5 & 0 & 0 \\ 0 & -0.5 & 0 \\ 0 & 0 & -0.55 \end{bmatrix} \tag{20}$$

$$B_{f2} = \begin{bmatrix} 0.5 \\ 0.5 \\ 0.55 \end{bmatrix}, \quad C_{f2} = \begin{bmatrix} 1 & 1 & 1 \end{bmatrix} \quad D_{f2} = 0_{3\times3} \tag{21}$$

For the implementation on the microcontroller, F_2 and F_3 were discretized via bilinear trasformation method with a sampling time of 0.2s. The signal x_3 was configured to output "1" when there is a drop-off, and "0" otherwise. The thresholds of $\epsilon = 30$, $\epsilon_l = \epsilon_u = 20$ have also been selected after the system calibrations.

In order to evaluate the performance via y_2, y_3 and y_4, six different experiments were structured as depicted in Figure 11 where Experiments 1,2,3,4,5 and 6 were represented by subfigures (a), (b), (c), (d), (e) and (f) respectively. The smart cane user is indicated by the blue circle whereas the static obstacle on the ground is denoted by the grey rectangle.

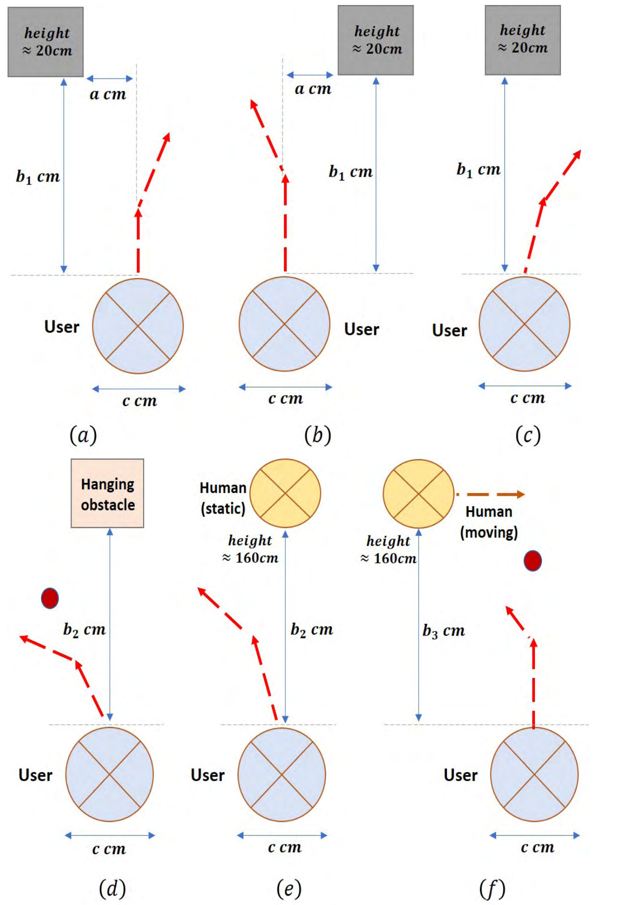

FIGURE 11. **Experiments for the obstacle avoidance performance evaluations; the user is represented by the blue circle and the static obstacle on the ground is represented by the grey rectangle. Expected drop-off areas are indicated by the small dark-red circles. The dashed red lines show the user's predefined walking path and direction (with speed approximately at $20cm/s$). The specified distances/length are $a = 50$, $b_1 = 120$, $b_2 = 150$, $b_3 = 130$ and $c = 45$. From left to right: (a) Obstacle on the left; (b) Obstacle on the right; (c) Obstacle at the center; (d) A hanging obstacle at the center; (e) A non-moving human as a high obstacle at the center; (f) A human walking from left to right at around $60cm/s$ as a moving obstacle.**

The dashed red lines show the user's predefined walking path and direction (with speed approximately at $20cm/s$). Figure 12 illustrates the side views for the experiments with obstacle on the ground and drop-off. The smart cane was attached to a 1.16m walking stick for a user with a height of 155cm. The angles θ_h, θ_m and θ_g (as depicted in Figure 4) were respectively fixed to 50°, 40° and 45°. For all the experiments, the user walked from the same starting point, and the obstacles were initially $b_j (j = 1, 2, 3)$ cm away from the user. Experiments 1, 2 and 3 were designed to analyse the obstacle detection performance when a static obstacle with a height of 20cm on the ground was placed on the left, right and at the center with respect to the user, whereas for a hanging obstacle (approximately at the user's head-level), static and moving humans, the performance were evaluated via Experiments 4,5 and 6 respectively. To test the controller's performance for S_g, the drop-off areas are included in Experiments 4 and 6 as indicated by the small dark-red circles.

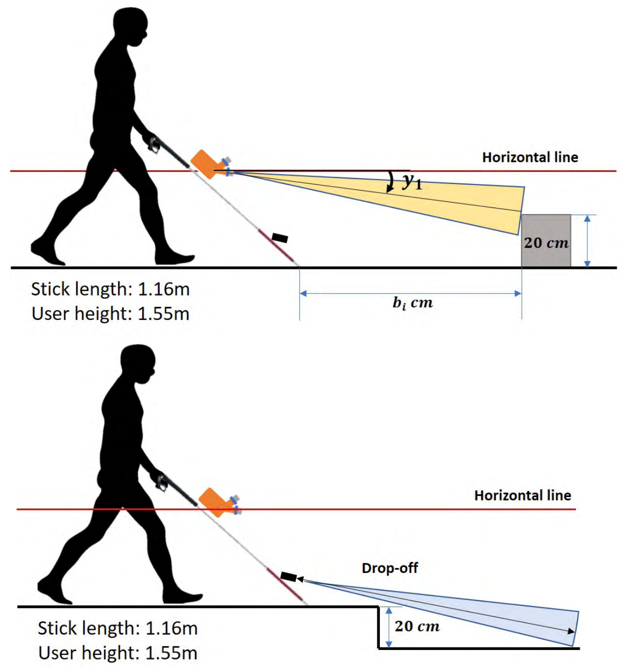

FIGURE 12. **Side views for experiments with obstacle on the ground (top) and drop-off (bottom).**

TABLE 5. **Performance evaluations from y_2, y_3 and y_4 responses via open-loop (OL) and Result 2 (R2.2).**

		Total Error (TE)					
y_i	Method	Exp 1	Exp 2	Exp 3	Exp 4	Exp 5	Exp 6
y_2	OL	6.22	12.9	28.0	48.7	109	24.5
	R2.2	1.79	6	14	30.9	79.4	5.8
y_3	OL	N/A	N/A	N/A	4	N/A	3
	R2.2	N/A	N/A	N/A	0.53	N/A	0.63
y_4	OL	9	10	15	N/A	15	N/A
	R2.2	2	2	2	N/A	2	N/A

Let $y_{ir} (i = 2, 3, 4)$ be the expected output signals of y_i where y_{2r} and y_{3r} are the desired user alerts for obstacle position and drop-off as in requirement (A1), and y_{4r} is the desired alert to satisfy (A2). Also, let y_{ib} denote y_i when Result 2 is applied, and y_{ix} be y_i produced via open-loop mode. The responses for y_i were recorded in Figures 13, 14, and 15 which also showed the corresponding x_i and β_i. From the figures, it was observed that the proposed method is able to significantly reduce the number of false alerts as can be seen from the responses of y_{ib} and y_{ix}. This was mainly due to the compensators F_i that produced filtered output β_i from the raw sensor signals x_i which usually suffered from the sudden drop-to-zero issues. With regard to Experiment 6 where another person was moving fastly from left to right at b_3 cm in front of the user, the proposed method was also capable to reduce the number of alerts as can be observed from the last column in Figure 14. This in turn satisfied the requirement in (A3).

The total error (TE) for quantitative performance evaluation of y_2 was calculated similar to the IAE as in (18), with

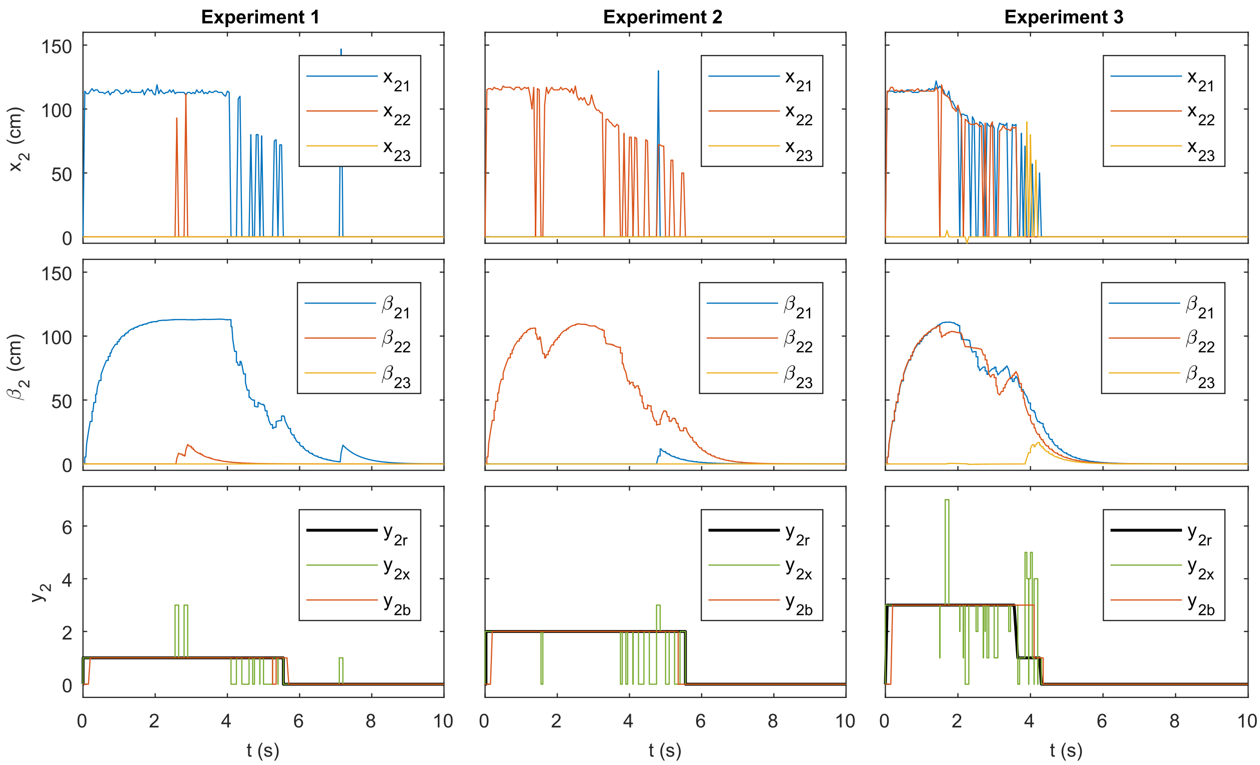

FIGURE 13. The responses of x_2, β_2 and y_2 for Experiments 1,2 and 3 are represented by the left, middle and right subfigures respectively.

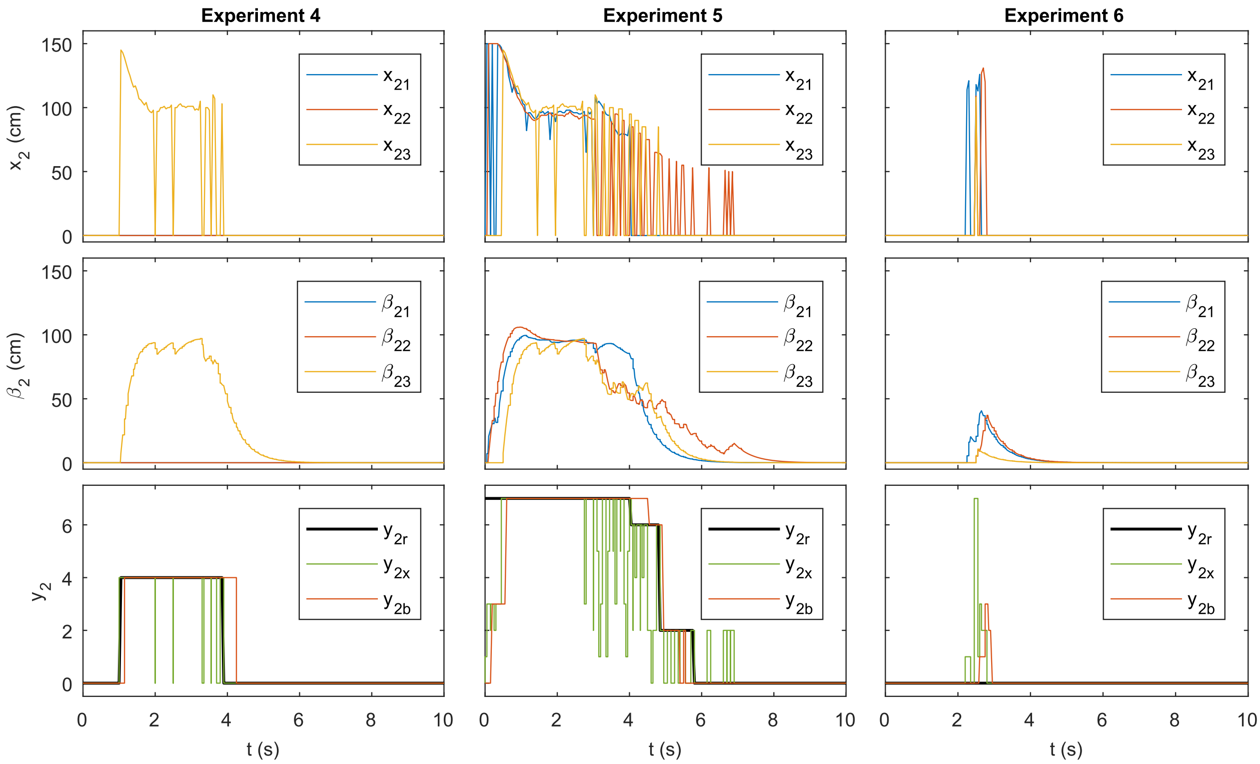

FIGURE 14. The responses of x_2, β_2 and y_2 for Experiments 4,5 and 6 are represented by the left, middle and right subfigures respectively.

y_1 and r_1 replaced by y_2 and y_{2r}. For y_3 and y_4, the TEs were evaluated slightly different than that for y_2 to accommodate the nature of u_{b3} and u_{b4} and suitability of the alerts to the user. To this end, let N_e be the the number of false readings,

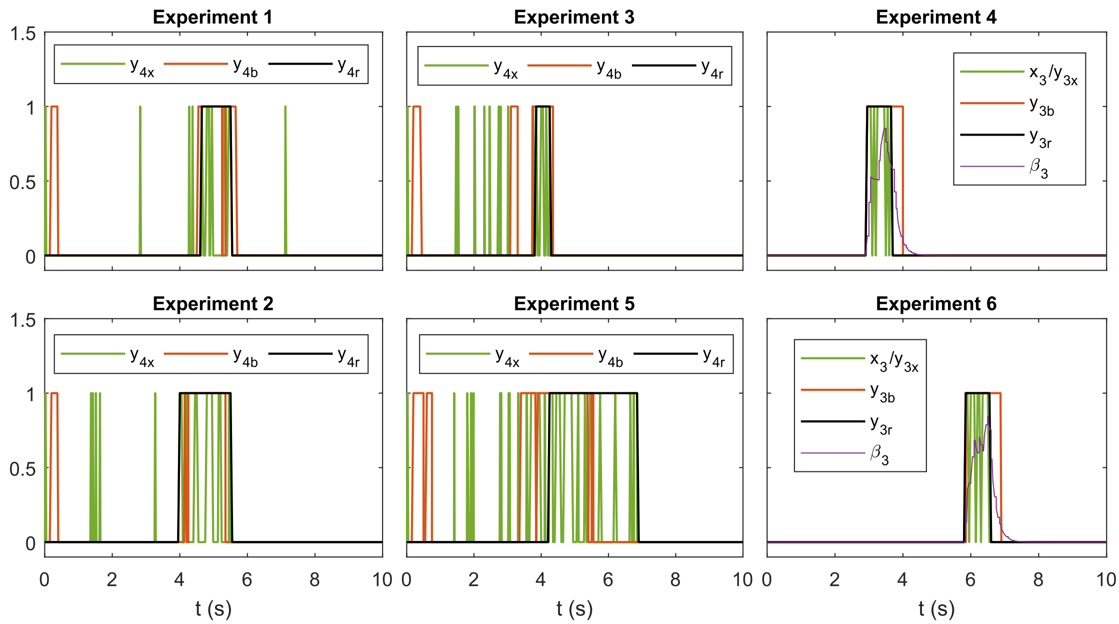

FIGURE 15. The responses of y_3 and y_4 for performance evaluations of requirement (A2) (via Experiments 1,2,3 and 5) and drop-off detection (via Experiments 4 and 6).

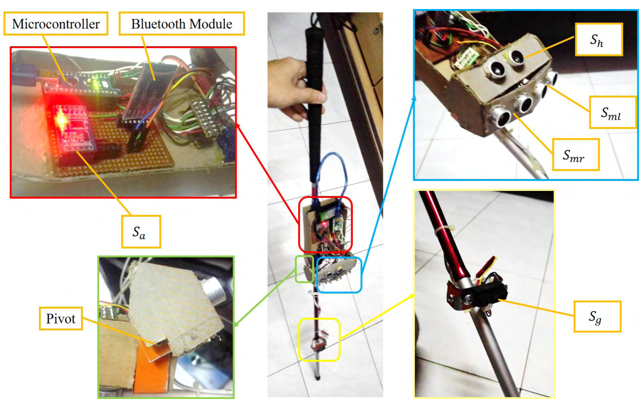

FIGURE 16. Prototype smart cane.

and τ_d be the delay between y_3 and y_{3r} in seconds. The corresponding TEs read

$$TE_{y_3} = \int_0^\infty (W_1 N_e + W_2 \tau_d) dt, \tag{22}$$

$$TE_{y_4} = \int_0^\infty W_1 N_e dt, \tag{23}$$

where $W_1 = 1$ and $W_2 = 0.5$ were the preferred weights. From the recorded results in Table 5, it is clearly seen that all the TEs via applications of Result 2 are significantly smaller than those via the open-loop method. Thus, the design requirement in (A4) was satisfied. The prototype smart cane that was tested throughout the experiments is shown in Figure 16 where the HC-SR04 ultrasonic sensors were used for S_h, S_{mr} and S_{ml}, the Sharp GP2Y0A21YK0F infrared sensor for S_g and MMA7361 accelerometer for S_a.

IV. DISCUSSIONS AND CONCLUSIONS

In this work, we have proposed a multi-sensor obstacle detection system for a smart cane via model-based state-feedback control strategy to regulate the detection angle of the sensors and minimize the false alerts to the user. The sensors' positions were further optimized via an LQR-based controller while the sensor signals sent to the users were filtered out via dynamic feedback compensators to minimize the false alerts. The effectiveness of the approach has been verified via the designed experiments, and the numerical results have shown that the proposed method can provide significant improvements over the conventional methods in terms of error reductions.

For future work, the techniques proposed can be adopted and modified to suit other ETAs with different designs such as the wearable assitive devices for the blinds. A survey among the visually challenged on the convenience of the prototype via several experiments may also be useful to enhance the usability of the device.

REFERENCES

[1] *Electronic Travel Aids: New Directions for Research*, Committee Vis.

[2] D. Dakopoulos and N. G. Bourbakis, "Wearable obstacle avoidance electronic travel aids for blind: A survey," *IEEE Trans. Syst., Man, Cybern. C, Appl. Rev.*, vol. 40, no. 1, pp. 25–35, Jan. 2010.

[3] W. Elmannai and K. Elleithy, "Sensor-based assistive devices for visually-impaired people: Current status, challenges, and future directions," *Sensors*, vol. 17, no. 3, p. 565, 2017.

[4] A. S. Al-Fahoum, H. B. Al-Hmoud, and A. A. Al-Fraihat, "A smart infrared microcontroller-based blind guidance system," *Active Passive Electron. Compon.*, vol. 2013, Jun. 2013, Art. no. 726480.

[5] B. Mustapha, A. Zayegh, and R. K. Begg, "Ultrasonic and infrared sensors performance in a wireless obstacle detection system," in *Proc. 1st Int. Conf. Artif. Intell., Modelling Simulation*, Dec. 2013, pp. 487–492.

[6] R. Pyun, Y. Kim, P. Wespe, R. Gassert, and S. Schneller, "Advanced augmented white cane with obstacle height and distance feedback," in *Proc. IEEE 13th Int. Conf. Rehabil. Robot. (ICORR)*, Jun. 2013, pp. 1–6.

[7] M. Dekan, D. František, B. Andrej, R. Jozef, R. Dávid, and M. Josip, "Moving obstacles detection based on laser range finder measurements," *Int. J. Adv. Robot. Syst.*, vol. 15, no. 1, pp. 1–18, 2018.

[8] S. V. F. Barreto R. E. Sant'Anna, and M. A. F. Feitosa, "A method for image processing and distance measuring based on laser distance triangulation," in *Proc. IEEE 20th Int. Conf. Electron., Circuits, Syst. (ICECS)*, Dec. 2013, pp. 695–698.
[9] R. Henderson and K. Schulmeister, *Laser Safety*. New York, NY, USA: Taylor & Francis, 2004.
[10] P. Chanana, R. Paul, M. Balakrishnan, and P. Rao, "Assistive technology solutions for aiding travel of pedestrians with visual impairment," *J. Rehabil. Assistive Technol. Eng.*, vol. 4, pp. 1–16, Aug. 2017.
[11] E. M. Ball, *Electronic Travel Aids: An Assessment*. London, U.K.: Springer, 2008, pp. 289–321.
[12] J. Liu, J. Liu, L. Xu, and W. Jin, "Electronic travel aids for the blind based on sensory substitution," in *Proc. 5th Int. Conf. Comput. Sci. Edu. (ICCSE)*, Aug. 2010, pp. 1328–1331.
[13] S. Kumpakeaw, "Twin low-cost infrared range finders for detecting obstacles using in mobile platforms," in *Proc. IEEE Int. Conf. Robot. Biomimetics (ROBIO)*, Dec. 2012, pp. 1996–1999.
[14] G.-Y. Jeong and K.-H. Yu, "Multi-section sensing and vibrotactile perception for walking guide of visually impaired person," *Sensors*, vol. 16, no. 7, p. 1070, 2016.
[15] F. Prattico, C. Cera, and F. Petroni, "A new hybrid infrared-ultrasonic electronic travel aids for blind people," *Sens. Actuators A, Phys.*, vol. 201, pp. 363–370, Oct. 2013.
[16] D. N. Hung, V. Minh-Thanh, N. Minh-Triet, Q. L. Huy, and V. T. Cuong, "Design and implementation of smart cane for visually impaired people," in *Proc. 6th Int. Conf. Develop. Biomed. Eng. Vietnam (BME6)*, T. V. Van, T. A. N. Le, and T. N. Duc, Eds. Singapore: Springer, 2018, pp. 249–254.
[17] S. Chaurasia and K. V. N. Kavitha, "An electronic walking stick for blinds," in *Proc. Int. Conf. Inf. Commun. Embedded Syst. (ICICES)*, Feb. 2014, pp. 1–5.
[18] R. K. Megalingam, A. Nambissan, A. Thambi, A. Gopinath, and M. Nandakumar, "Sound and touch based smart cane: Better walking experience for visually challenged," in *Proc. IEEE Canada Int. Humanitarian Technol. Conf. (IHTC)*, Jun. 2014, pp. 1–4.
[19] D. Kim, K. Kim, and S. Lee, "Stereo camera based virtual cane system with identifiable distance tactile feedback for the blind," *Sensors*, vol. 14, no. 6, pp. 10412–10431, 2014.
[20] D. R. Chebat, S. Maidenbaum, and A. Amedi, "Navigation using sensory substitution in real and virtual mazes," *PLoS ONE*, vol. 10, no. 6, pp. 1–18, Jun. 2015.
[21] S. Shoval, J. Borenstein, and Y. Koren, "Mobile robot obstacle avoidance in a computerized travel aid for the blind," in *Proc. IEEE Int. Conf. Robot. Autom.*, vol. 3, May 1994, pp. 2023–2028.
[22] I. Ulrich and J. Borenstein, "The GuideCane-applying mobile robot technologies to assist the visually impaired," *IEEE Trans. Syst., Man, Cybern. A, Syst., Humans*, vol. 31, no. 2, pp. 131–136, Mar. 2001.
[23] A. Rodrìguez, J. J. Yebes, P. F. Alcantarilla, L. M. Bergasa, J. Almazán, and A. Cela, "Assisting the visually impaired: Obstacle detection and warning system by acoustic feedback," *Sensors*, vol. 12, no. 12, pp. 17476–17496, 2012.
[24] A. S. Martinez-Sala, F. Losilla, J. C. Sánchez-Aarnoutse, and J. Garcia-Haro, "Design, implementation and evaluation of an indoor navigation system for visually impaired people," *Sensors*, vol. 15, no. 12, pp. 32168–32187, 2015.
[25] D. Nakamura, H. Takizawa, M. Aoyagi, N. Ezaki, and S. Mizuno, "Smartphone-based escalator recognition for the visually impaired," *Sensors*, vol. 17, no. 5, p. 1057, 2017.
[26] B.-S. Lin, C.-C. Lee, and P.-Y. Chiang, "Simple smartphone-based guiding system for visually impaired people," *Sensors*, vol. 17, no. 6, p. 1371, 2017.
[27] U. R. Roentgen, G. J. Gelderblom, M. Soede, and L. P. de Witte, "Inventory of electronic mobility aids for persons with visual impairments: A literature review," *J. Vis. Impairment Blindness*, vol. 102, no. 11, pp. 702–724, 2008.
[28] S. Y. Kim and K. Cho, "Usability and design guidelines of smart canes for users with visual impairments," *Int. J. Des.*, vol. 7, no. 1, pp. 99–110, 2013.
[29] A. G. Abdel-Wahab and A. A. A. El-Masry, *Mobile Information Communication Technologies Adoption in Developing Countries: Effects and Implications*. Hershey, PA, USA: IGI Global, 2011.
[30] K. Ogata, *Modern Control Engineering*, 4th ed. Upper Saddle River, NJ, USA: Prentice-Hall, 2001.

NUR SYAZREEN AHMAD (M'14) was born in Kuala Lumpur, Malaysia. She received the B.Eng. degree (Hons.) in electrical and electronic engineering and the Ph.D. degree in control systems from The University of Manchester, U.K., in 2009 and 2012, respectively. She became a member of the IEEE Control Systems Society in 2014.

Since 2013, she has been with the School of Electrical and Electronic Engineering, Universiti Sains Malaysia. Her research work centers around motion control, robust stability and performance analysis of constrained and nonlinear systems, and optimization-based controller synthesis with linear matrix inequality searches. Her current research interest includes phase-locked loops, embedded control systems, and robust control analysis, and design of autonomous mobile systems.

NG LAI BOON was born in Butterworth, Malaysia, in 1992. He received the B.Eng. degree (Hons.) in electronic engineering from Universiti Sains Malaysia in 2017. He is currently with Intel, Penang, and pursuing a part-time M.Sc. degree in electrical engineering (computer and microelectronic systems) with Universiti Teknologi Malaysia. He is currently with Intel, Penang, Malaysia.

PATRICK GOH received the B.S., M.S., and Ph.D. degrees in electrical engineering from the University of Illinois at Urbana–Champaign, Champaign, IL, USA in 2007, 2009, and 2012 respectively.

Since 2012, he has been with the School of Electrical and Electronic Engineering, Universiti Sains Malaysia, where he currently specializes in the study of signal integrity for high-speed digital designs. His research interest includes the development of circuit simulation algorithms for computer-aided design tools. He was a recipient of the Raj Mittra Award in 2012 and the Harold L. Olesen Award in 2010, and has served on the technical program committee and international program committee in various IEEE and non-IEEE conferences around the world.